Chem. Eng. Comm. 1989, Vol. 85, pp. 85–94
Reprints available directly from the publisher.
Photocopying permitted by license only.

Printed in the United States of America

6-B

ANALYSIS OF HEAT PIPE VAPOR DYNAMICS

F. ISSACCI, I. CATTON, A. HEISS, and N.M. GHONIEM

Mechanical, Aerospace and Nuclear Engineering Department
University of Los Angeles
Los Angeles, California 90024-1597

(Received September 29, 1988; in final form March 22, 1989)

The transient behavior of vapor flow in heat pipes is analyzed numerically using a two dimensional compressible flow model. The vapor core response to changes in the evaporation and condensation rates following a sudden increase, or decrease, in the input heat flux, or the condensation temperature is studied. The numberical scheme is fully implicit using a staggered grid to overcome the numerical stability problem. When the input heat flux is low, the vapor flows smoothly towards the condensation region. However, with high input heat flux, reverse flow was detected in the adiabatic as well as the condensation region.
KEYWORDS Heat pipe Vapor Dynamics Analysis.

1. INTRODUCTION

In thermal systems in which a heat pipe is used as a device to conduct a huge amount of heat in a short time, the question "How much, how fast?" is the main issue in designing such systems. In studies of dynamic behavior of heat pipes, three different areas of concern are startup, shut down and operational transients. Intensive studies have been carried out at the Los Alamos National Laboratory on startup and shut down operations of heat pipes (Merrigan, 1985 and 1986; Merrigan *et al.*, 1986; and Costello *et al.*, 1986). Although the major part of these studies is experimental, a numerical analyses has been carried out using a simple one-dimensional model (Costello *et al.*, 1986). Bystrov and Goncharov (1983) and Ambrose *et al.*, (1987) have studied the starting dynamics of high temperature gas filled heat pipes experimentally and numerically.

The works done so far on transient behavior of heat pipes, mainly concern the startup and shut down operations and the analysis are carried out mostly on a one-dimensional model. In studies carried out at the Moscow Energy Institute on gas-controlled heat pipes (Galaktionov *et al.*, 1982; Galaktionov and Trukhanova, 1985), the temperature profiles under steady state conditions show that the radial and axial components of temperature are quite comparable. This clearly demonstrates the two dimensional character of the problem.

The flow patterns in a heat pipe are shown in Figure 1. The working liquid evaporates in evaporation zone. The local pressure increases and the vapor flows towards the condensation zone, at which it condenses back to the liquid phase. The liquid flows from the condenser to the evaporator by capillary force through the wick structure. In this work, the transient behavior of vapor flow is analyzed

75

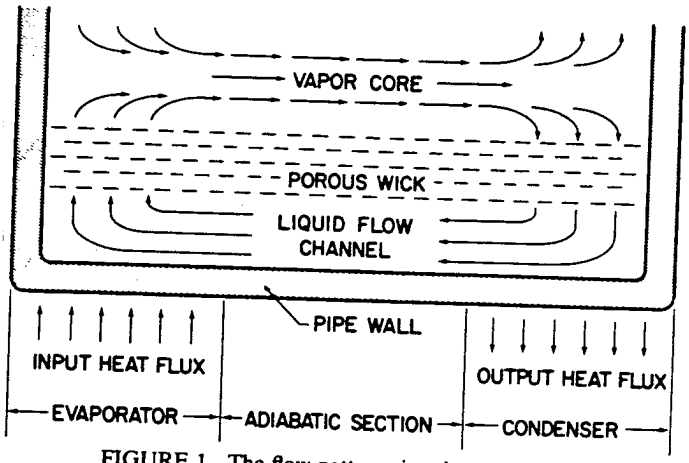

FIGURE 1 The flow patterns in a heat pipe.

numerically using a two dimensional model. The main concern is the vapor core response to changes in the evaporation and condensation rates due to a sudden increase, or decrease, in the input heat flux, or the condensation temperature.

2. GOVERNING EQUATIONS

The vapor flow in the heat pipe core, shown in Figure 1, is modeled as the channel flow shown in Figure 2. The equations governing the vapor flow are the time dependent, viscous, compressible, two-dimensional momentum, continuity, and energy conservation equations. The ideal gas law is used to relate pressure, density and temperature within the vapor core. These equations in Cartesian

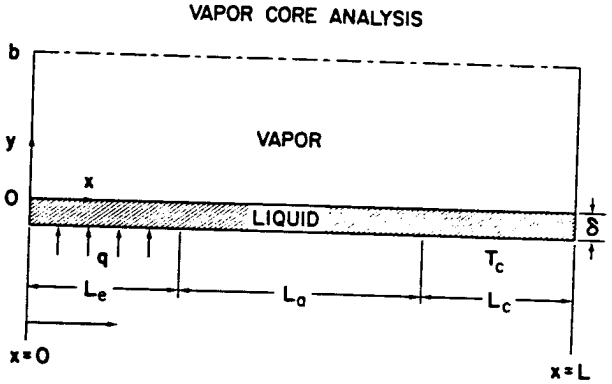

FIGURE 2 The vapor core model of the heat pipe.

coordinates are

Continuity

X-Momentum

$$\frac{\partial(\rho u)}{\partial t}+\frac{\partial(\rho uu)}{\partial x}+\frac{\partial(}{}$$

Y-Momentum

$$\frac{\partial(\rho v)}{\partial t}+\frac{\partial(\rho uv)}{\partial x}+\frac{\partial(}{}$$

Energy

$$c_p\left[\frac{\partial(\rho T)}{\partial t}+\frac{\partial(\rho uT)}{\partial x}\right.$$

State

2.1 Boundary Cond

The boundaries of th
for velocity compone
the side walls. These

@

At the center line the

The boundary condit

coordinates are

Continuity

$$\frac{\partial(\rho)}{\partial t}+\frac{\partial(\rho u)}{\partial x}+\frac{\partial(\rho v)}{\partial y}=0 \tag{1}$$

X-Momentum

$$\frac{\partial(\rho u)}{\partial t}+\frac{\partial(\rho uu)}{\partial x}+\frac{\partial(\rho vu)}{\partial y}=-\frac{\partial p}{\partial x}+\frac{\partial}{\partial x}\left(\mu\frac{\partial u}{\partial x}\right)+\frac{\partial}{\partial y}\left(\mu\frac{\partial u}{\partial y}\right)$$
$$+\left\{\frac{\partial}{\partial x}\left(\mu\frac{\partial u}{\partial x}\right)+\frac{\partial}{\partial y}\left(\mu\frac{\partial v}{\partial x}\right)-\frac{2}{3}\frac{\partial}{\partial x}\left(\mu\frac{\partial u}{\partial x}+\mu\frac{\partial v}{\partial y}\right)\right\} \tag{2}$$

Y-Momentum

$$\frac{\partial(\rho v)}{\partial t}+\frac{\partial(\rho uv)}{\partial x}+\frac{\partial(\rho vv)}{\partial y}=-\frac{\partial p}{\partial y}+\frac{\partial}{\partial x}\left(\mu\frac{\partial v}{\partial x}\right)+\frac{\partial}{\partial y}\left(\mu\frac{\partial v}{\partial y}\right)$$
$$+\left\{\frac{\partial}{\partial x}\left(\mu\frac{\partial u}{\partial y}\right)+\frac{\partial}{\partial y}\left(\mu\frac{\partial v}{\partial y}\right)-\frac{2}{3}\frac{\partial}{\partial y}\left(\mu\frac{\partial u}{\partial x}+\mu\frac{\partial v}{\partial y}\right)\right\} \tag{3}$$

Energy

$$c_p\left[\frac{\partial(\rho T)}{\partial t}+\frac{\partial(\rho uT)}{\partial x}+\frac{\partial(\rho vT)}{\partial y}\right]=\frac{\partial}{\partial x}\left(k\frac{\partial T}{\partial x}\right)+\frac{\partial}{\partial y}\left(k\frac{\partial T}{\partial y}\right)+\frac{\partial p}{\partial t}+u\frac{\partial p}{\partial x}+v\frac{\partial p}{\partial y}$$
$$+\mu\left[2\left(\frac{\partial u}{\partial x}\right)^2+2\left(\frac{\partial v}{\partial y}\right)^2+\left(\frac{\partial u}{\partial y}\right)^2+\left(\frac{\partial v}{\partial x}\right)^2\right] \tag{4}$$

State

$$p=R\rho T \tag{5}$$

2.1 *Boundary Conditions*

The boundaries of the vapor core are shown in Figure 2. The nonslip condition for velocity components and adiabatic condition for temperature are assumed on the side walls. These conditions are formulated as

$$@\ x=0 \quad \text{and } L, \qquad u=v=0 \qquad \frac{\partial T}{\partial x}=0 \tag{6}$$

At the center line the symmetry condition implies,

$$@\ y=b, \qquad \frac{\partial u}{\partial y}=0$$
$$v=0$$
$$\frac{\partial T}{\partial y}=0 \tag{7}$$

The boundary conditions on the liquid side are the challenging ones. The liquid

flow is assumed in a porous medium with thickness δ, which is much smaller than the vapor thickness, b. The axial velocity is zero on this boundary. That is,

$$@\ y = 0, \qquad u = 0 \tag{8}$$

In order to assign boundary conditions for the vertical velocity and temperature, the liquid–vapor interface boundary is divided to three regions. At the evaporation zone the input heat flux, q, is a given parameter and the input flow is approximated as

$$\rho v = \dot{m} \approx q / H_{fg}(T) \tag{9}$$

In the above equation, H_{fg} is the heat of vaporization and conduction in the liquid layer is ignored. The temperature is assumed to be the saturation temperature of the liquid corresponding to the system pressure. That is

$$T = T_{sat}(p) \tag{10}$$

In the adiabatic zone the boundary conditions are

$$v = 0 \qquad \frac{\partial T}{\partial y} = 0 \tag{11}$$

In the condensation zone the temperature, T_c, is a given parameter and the output flow is approximated as

$$\rho v = \dot{m} \approx -\frac{k_{eff}}{\delta}\left(\frac{T - T_c}{H_{fg}(T)}\right) \tag{12}$$

$$T = T_{sat}(p) \tag{13}$$

where k_{eff} is the effective conductivity of the liquid layer.

3. SOLUTION METHOD

Equations (1) to (5) are five equations for five unknowns, namely, ρ, u, v, T and p. The boundary conditions associated with these equations are Eqs. (6) to (13). The boundary conditions on the vapor–liquid interface depend on the pressure and pressure is not available on the boundaries. However, in the numerical method described below, the pressure does not need to be specified on the boundaries. The method used here is based on the SIMPLE method described by Patankar (1980). In this method all the variables are not calculated for the same grid points. The staggered grid is shown in Figure 3. The velocity components are calculated for the points that lie on the faces of the control volumes. The locations for u and v are shown by short arrows in the figure. The other dependent variables, namely ρ, T and p, are calculated for the main grid points shown by small circles. The time dependent terms in the governing equations were discretisized using the backward Euler method while the power law scheme was used for differencing the convective terms.

The algorithm for calculation is the following: The pressure is assumed to be

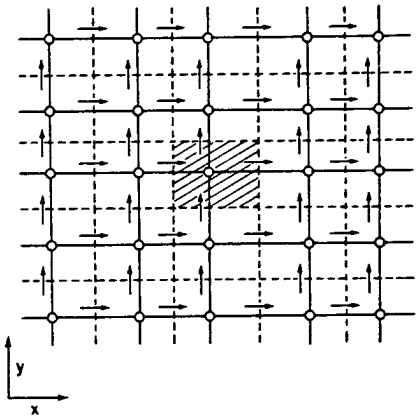

FIGURE 3 Staggered grid. → locations for u, ↑ locations for v, • locations for ρ, T and p.

composed of two parts

$$p(x, y, t) = \bar{p}(t) + \tilde{p}(x, y, t) \tag{14}$$

where $\bar{p}(t)$ is the space averaged system pressure and $\tilde{p}(x, y, t)$ includes the space variation of the pressure. Assuming a pressure distribution, the momentum equations are solved for u and v. Then using the continuity equation and the density, ρ, from the last iteration on temperature, the pressure is corrected to be used in momentum equations again. Upon accomplishing these iterations, the velocity fields and $\tilde{p}$ will be found.

The energy equation is then solved for temperature. In order to calculate density from the equation of state and to evaluate the boundary conditions, we need the absolute value of the pressure term. Global mass balance is used to calculate the absolute pressure. The total mass, m, is related to the pressure by

$$m = \int_V \rho \, dV = \int_V \frac{p}{RT} dV \tag{15}$$

The increase in the total mass in one time step is

$$m(t + \Delta t) - m(t) = (\dot{m}_{in} - \dot{m}_{out})\Delta t \tag{16}$$

where $\dot{m}_{in}$ and $\dot{m}_{out}$ are the input and output mass fluxes, respectively, and are found from the boundary conditions. Equations (15) and (16) are combined to yield

$$(\dot{m}_{in} - \dot{m}_{out})\,\Delta t = \int_V \left[\frac{P|_{t+\Delta t}}{RT|_{t+\Delta t}} - \frac{P|_t}{RT|_t} \right] dV \tag{17}$$

Thus, Eq. (17) is used to evaluate the absolute pressure of the system.

4. RESULTS

The computational procedure described above was implemented and computations were done for several evaporator heat fluxes for water as a working fluid.

Unfortunately, there is no experimental data available to compare the computational results. The pipe dimensions used in the calculations were $b = 2.5$ cm and $L = 3b$, and the computational grid spacings were $\Delta x = 0.1$ and $\Delta y = 0.05$. The temperature and pressure variations, and consequently, the density variation, were found to be quite small inside the pipe. This is expected of systems in which condensation occurs without a non-condensible gas. Steady state results are shown in Figures 4, 5 and 6. The steady state was assumed to be reached when the relative change of all variables within a time step was less than 0.5%. Figures 4 show the axial velocity profiles at different axial cross sections along the pipe, for low input heat flux, Figure 4(a), and for high input heat flux, Figure 4(b) The flow stream lines for these two cases are shown schematically in Figures 5.

When the input heat flux is relatively low, the evaporation rate is low and the vapor flows smoothly towards the condensation region (Figures 4(a) and 5(a)). However, with high input heat flux the evaporation rate is high, the vapor is ejected with a high momentum from the evaporator and condenses at a high rate at condenser. This high momentum flow at two ends of the adiabatic section causes a circulation flow in this region. That is, on the adiabatic surface there is a reverse flow. In addition, in the condensation region the high momentum vapor flow impacts the rigid end wall, returns and then condenses in the liquid region.

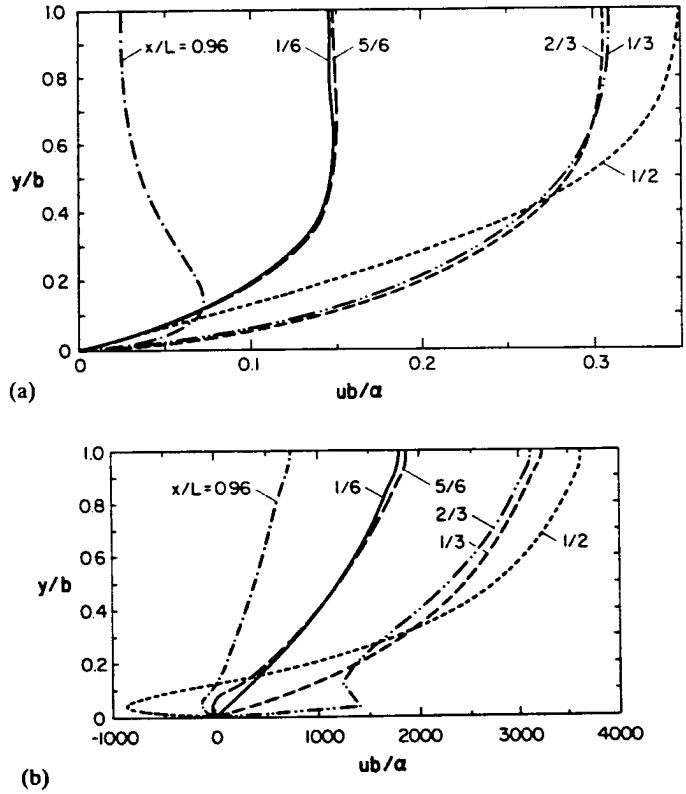

FIGURE 4 Axial velocity profiles, (a) low input heat flux ($Re = 1.0$), (b) high input heat flux ($Re = 1000$).

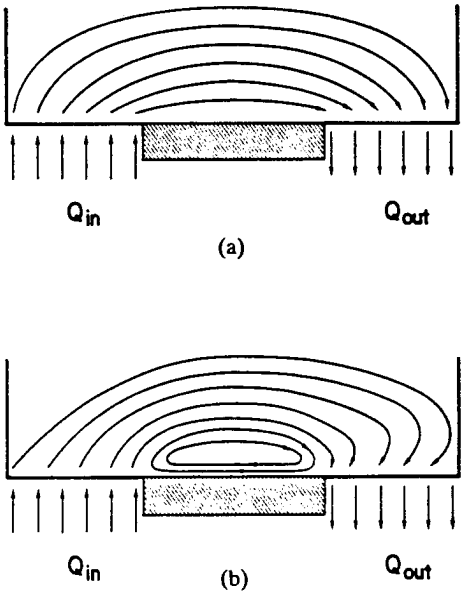

FIGURE 5 Vapor flow patterns: (a) low input heat flux, (b) high input heat flux.

This return flow is shown in Figures 4(b) and 5(b). The vertical velocity profiles for different vertical cross sections are shown in Figure 6. The flow is clearly two-dimensional.

Reverse flow in heat pipes with high input heat flux is both physically and mathematically valid. Further, Galaktionov and Trukhanova (1985) observed a reverse flow in the gas-controlled heat pipe. The reversed flow solution in the paper was obtained by using the solution for a low input heat flux (no reverse flow) as an initial condition then raised the input heat flux at the evaporator. It has been shown by Serrin (1959) that the Navier–Stokes equations have a unique solution if they are considered as an initial value problem. Therefore the reversed flow is both unique and a valid solution for a high input heat flux.

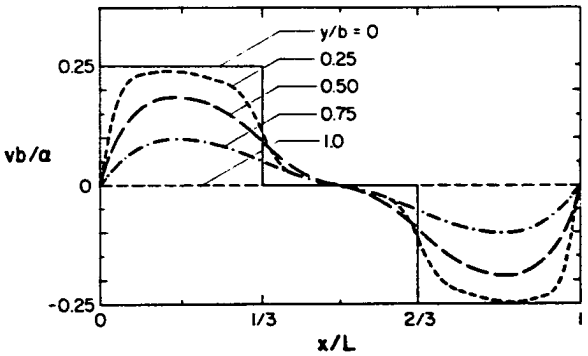

FIGURE 6 Vertical velocity profiles.

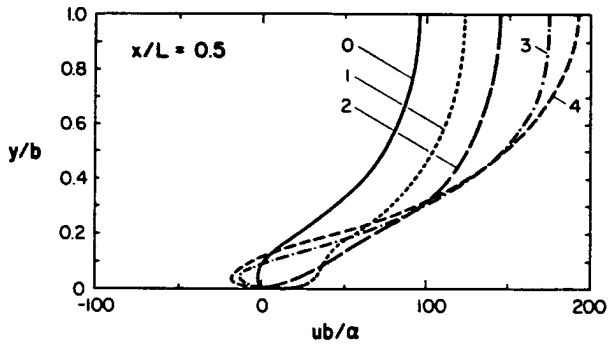

FIGURE 7 Axial velocity profile at different time steps. O-Initial profile ($\tau = 0$), $1 - \tau = 10^{-4}$, $2 - \tau = -2.5 \times 10^{-3}$, $3 - \tau = 10^{-2}$, 4-steady state ($\tau = 2.5 \times 10^{2}$) where $\tau = t\alpha/b^2$.

Transient behavior of vapor flow was studied using a steady state solution as the initial condition for different input parameters. As an example, Figure 7 shows the axial velocity profile at the middle of the pipe, $x/L = 1.5$, at different time steps. Curve 0 on this figure is the steady state solution for $Re = 100$, where Reynolds number is defined as

$$Re = \frac{\dot{m}_{in} b}{\mu}$$

and $\dot{m}_{in}$ is the input mass flux. Curves 1 to 4 show this velocity profile at different time steps after a sudden increase in input heat flux for $Re = 200$. At the outset, the increase in input heat flux overcomes the reverse flow, see curve 1. As the velocity profile develops with time, the steady state profile, curve 4, shows a higher reverse flow at the liquid–vapor interface.

5. CONCLUSIONS

The dynamic behavior of the vapor flow in heat pipes was studied for transient operations. Although the solution is presented for Cartesian coordinates, the computational code can be easily modified for the circular heat pipes. Interesting phenomena have been detected in the adiabatic and condensation regions. In these sections high input heat flux may cause a reverse flow. The inverse flow means the negative shear force on the wick structure. Here one must wonder how relevant the entrainment limit is. Further, in transient operations the shear force at one location may change sign. Detailed information on shear force is needed for design purposes, and this needs a proper two-dimensional analysis.

ACKNOWLEDGMENT
This work was performe
Office of the Strategic
DNA 001-C-0320. The w
No. NAG3-899 and NAS

NOMENCLATURE

b	Channel width
c_p	Specific heat
H_{fg}	Latent heat
k	Conductivity
k_{eff}	Effective conduc
L	Channel length
m	Total mass
$\dot{m}$	Mass flux
$\dot{m}_{in}$	Input mass flux
$\dot{m}_{out}$	Output mass flu
p	Pressure
$\bar{p}$	Average pressu
$\tilde{p}$	Pressure deviati
Pr	Prandtl number
q	Input heat flux
R	Gas constant
Re	Reynolds numb
t	Time
T	Temperature
T_c	Condenser tem
T_{sat}	Saturation tem
u	Axial velocity
v	Vertical velocit
V	Volume
x	Axial coordinat
y	Vertical coordi
δ	Liquid layer th
α	Thermal diffusi
μ	Viscosity
ρ	Density
τ	Fourier numbe

al profile ($\tau = 0$), $1 - \tau = 10^{-4}$,
e $\tau = t\alpha/b^2$.

a steady state solution as
as an example, Figure 7
e, $x/L = 1.5$, at different
ition for $Re = 100$, where

locity profile at different
$Re = 200$. At the outset,
ow, see curve 1. As the
ofile, curve 4, shows a

as studied for transient
tesian coordinates, the
heat pipes. Interesting
ndensation regions. In
flow. The inverse flow
e one must wonder how
erations the shear force
n shear force is needed
nal analysis.

ACKNOWLEDGMENT

This work was performed partly for the Innovative Science and Technology Office of the Strategic Defense Initiative Organization under Contract No. DNA 001-C-0320. The work was also supported by NASA Lewis under Contract No. NAG3-899 and NASA Dryden under Contract No. NCC2-374 Supp 2.

NOMENCLATURE

b	Channel width
c_p	Specific heat
H_{fg}	Latent heat
k	Conductivity
k_{eff}	Effective conductivity of liquid layer
L	Channel length
m	Total mass
$\dot{m}$	Mass flux
$\dot{m}_{\text{in}}$	Input mass flux
$\dot{m}_{\text{out}}$	Output mass flux
p	Pressure
$\bar{p}$	Average pressure
$\tilde{p}$	Pressure deviation from the averaged pressure
Pr	Prandtl number
q	Input heat flux
R	Gas constant
Re	Reynolds number
t	Time
T	Temperature
T_c	Condenser temperature
T_{sat}	Saturation temperature
u	Axial velocity
v	Vertical velocity
V	Volume
x	Axial coordinate
y	Vertical coordinate
δ	Liquid layer thickness
α	Thermal diffusivity
μ	Viscosity
ρ	Density
τ	Fourier number

REFERENCES

Ambrose, J.H., Chow, L.C., and Beam, J.E., 1987. "Transient Heat Pipe Response and Rewetting Behavior," *Journal of Thermophysics*, **1**, No. 3, pp. 222–227.

Bystrov, P.I., and Goncharov, V.F., 1983, "Starting Dynamics of High-Temperature Gas-Filled Heat Pipes," *High Temperature*, **21**, No. 6, pp. 927–936.

Costello, F.A., Montague, A.F., and Merrigan, M.A., 1986, "Detailed Transient Model of a Liquid-Metal Heat Pipe," *Proceedings, AIAA/ASME 4th Joint Thermophysics and Heat Transfer Conference*, Boston, MA.

Galaktionov, V.V., Parfent'eva, A.A., Partnov, D.V., and Sasin, V.Ya, 1982, "Vapor-Gas Front in the Condenser of a Two-Dimensional Gas-Controlled Heat Pipe," *J. Eng. Phys*, **42**, pp. 273–277.

Galaktionov, V.V., and Trukhanova, 1985, "Study of the Process of Heat and Mass Transfer in the Region of the Vapor-Gas Front in a Gas-Regulable Heat Pipe," *J. Eng. Physics*, **48**, pp. 296–300.

Merrigan, M.A., 1985, "Heat Pipe Technology Issues," Proceedings, 1st Symposium on Space Nuclear Power Systems, M.S. El-Genk and M.D. Hooever, ed., Orbit Book Co., Florida, pp. 419–426.

Merrigan, M.A., 1986, "Heat Pipe Design for Space Power Heat Rejection Applications," Proceedings, 21st Intersociety Energy Conversion Conference, pp. 1993–1998.

Merrigan, M. A., Keddy, E.S., and Sena, J. T., 1986, "Transient Performance Investigation of a Space Power System Heat Pipe," *Proceedings*, AIAA/ASME 4th Joint Thermophysics and Heat Transfer Conference, Boston, MA.

Patankar, S.V., 1980, *Numerical Heat Transfer and Fluid Mechanics*, Hemispherical Publishing Co., NY.

Serrin, J., 1959, "On the Stability of Viscous Fluid Motions," *Arch. Rational Mech. Anal.*, **1**, pp. 1–13.

Chem. Eng. Comm. 1989, V
Reprints available directly fr
Photocopying permitted by li

FRAGME

VASILIS N.

(Rece

The problem of fragmentatic
mutually perpendicular bunc
The evolution of fragmen
procedure which rests in usi
to identify fragments and de
show that fragmentation occ
values. This observation is
fragmentation in 2- and 3-b
consisting of a single bundle
KEYWORDS Pore structu
Monte Carlo simulation.

1. INTRODUCTIO

Fragmentation of soli
since it is related to i
tion, gasification, and
responsible for, *inter*
particulate effluents (
emission of submicron
systems (Sundback *et*

Particle fragmentati
tally evidenced throug
of bituminous coal an
of char particles follo
also been inferred fr
fluidized beds, char
1984), or from transie
effluent CO_2 during b
et al., 1984)).

Attempts to accour

† Author to whom corres